Lawrence Berkeley National Laboratory

Title
Progress in durability of metal-supported solid oxide fuel cells with infiltrated electrodes

Permalink
https://escholarship.org/uc/item/6tf6s609

Authors
Dogdibegovic, Emir
Wang, Ruofan
Lau, Grace Y
et al.

Peer reviewed

Progress in Durability of Metal-Supported SOFCs with Infiltrated Electrodes

Emir Dogdibegovic[1]*, Ruofan Wang[1], Grace Y. Lau[1], Alireza Karimaghaloo[2],

Min Hwan Lee[2], and Michael C. Tucker[1]*

[1]Lawrence Berkeley National Laboratory, Energy Storage and Distributed

Resources Division,   1 Cyclotron Rd., MS 62-203, Berkeley, CA

94720, United States

[2] Department of Mechanical Engineering, University of California, Merced,

5200 North Lake Rd., Merced, CA 95343, United States

*Corresponding authors:

Emir Dogdibegovic, Edogdibegovic@lbl.gov, Tel 1 (510)486-5635, Mail stop

62-R0313, 1 Cyclotron Road, Berkeley, CA 94720, United States

Michael C. Tucker, MCTucker@lbl.gov, Tel +1 (510)486-5304, Mail stop 62-

R0203, 1 Cyclotron Road, Berkeley, CA 94720, United States

Abstract

High power density and longevity are required to commercialize solid oxide

fuel cells for vehicular applications. In this work, electrochemical durability of

high-performance metal-supported solid oxide fuel cells (MS-SOFCs) with

infiltrated catalysts is investigated. Durability screening of various cathode

and anode compositions is conducted. The Pr_6O_{11} cathode and $SDCN_{40}$ (40 vol

% Ni-60 vol% SDC) anode are selected due to preferential tradeoff between

performance and durability. X-ray diffraction indicates the catalyst phases

are stable after prolonged thermal annealing. Electrochemical impedance and scanning electron microscopy analyses show that the evolution of $SDCN_{40}$ is minimal, and coarsening and Cr poisoning of the Pr_6O_{11} catalyst are the dominant degradation mechanisms. These degradation mechanisms are addressed by implementing three additional fabrication steps: (1) preoxidation of the metal support, (2) deposition of thin and protective atomic layer deposition (ALD) coatings throughout the cathode-side electrode and support, and (3) *in situ* pre-coarsening of the catalysts. A favorable tradeoff is achieved: the combination of the three fabrication steps reduces degradation rate at 0.7 V and 700 ºC by two orders of magnitude to 2.3% kh^{-1}, while sacrificing 35% of initial power density. The catalyst pre-coarsening step is primarily responsible for the loss of performance.

Keywords: Solid oxide fuel cell; Metal-support; Degradation; Chromium poisoning; ALD coating; Preoxidation

Introduction

The symmetric-architecture metal supported solid oxide fuel cells (MS-SOFCs) developed at Lawrence Berkeley National Laboratory (LBNL) [1-3], with thin ceramic backbones and electrolyte layer sandwiched between low-cost stainless steel supports, provide a number of advantages over all-ceramic SOFCs. These advantages include mechanical ruggedness, excellent tolerance to thermal [4] and redox cycling (critical in cases of disruption, intermittent fuel supply [5], or thermal fluctuations following load changes)

[6], and extremely fast start-up capability [2, 7-11]. Furthermore, the majority of the cell is an inexpensive FeCr-based ferritic stainless steel and only a single co-sintering step is required, which can significantly reduce the materials and fabrication cost.

In our recent reports, the challenges of co-processing of the metal support and zirconia backbone structure in a single reducing-environment sintering step were addressed [2, 7, 12]. Matched thermal expansion and sintering shrinkage, good bonding and chemical compatibility between the cell components, and low oxidation rate suitable for the long lifetimes in stationary and mobile SOFC power plants have been demonstrated [2, 7, 12]. It is desirable to operate MS-SOFCs in the temperature range of 650-700 °C, where a suitable tradeoff between performance and longevity is achieved. Higher operating temperature may lead to: (1) rapid oxidation of the metal support ($\geq$800 °C) [2, 3], (2) accelerated Cr poisoning of the cathode catalyst [2, 13-15], and (3) rapid catalyst coarsening [16]. Lower operating temperature constrains the power density. Due to these challenges, progress in MS-SOFC peak power density has been rather stagnated, remaining typically between 50 and 500 mW cm^{-2} in the temperature range of 650 °C to 850 °C [11, 17-24]. Small passenger vehicles, however, require high power due to limited volume to house the MS-SOFC stack, and immediate response during rapid vehicular acceleration and transient driving conditions, such as intermittent fuel flow and continuous load variation.

In our preceding report [25], the cell specification (catalyst precursor chemistry, thickness of each cell layer, cell sintering conditions, backbone porosity, and catalyst firing temperature) was optimized, and YSZ electrolyte was replaced with higher-conductivity and thinner 10Sc1CeSZ (SCSZ). Infiltrating catalysts after cosintering the metal support and zirconia layers ensures high performance. With Pr_6O_{11} cathode catalyst and SDC 60vol%-Ni 40vol% ($SDCN_{40}$) anode catalyst, power density of 1.56 W cm^{-2} at 700 ºC in 3% humidified hydrogen was achieved.

Following substantial progress in improving performance [25], in this work we focus on increasing the longevity of MS-SOFCs. The expected lifetime of MS-SOFC stacks in vehicles is ~10,000 h; hence, fabrication of high performing and durable cells is crucial for commercialization of this technology. Premature degradation of anode-supported, all-ceramic SOFCs with steel stack components has been studied in great detail in the past few decades. Attempts to suppress Cr transport and cathode Cr poisoning were implemented through a variety of conductive/protective coatings of interconnectors [15, 26, 27], surface treatments and modifications (for example, Co-Mn spinels [33]), and alloy developments [26-32]. Different compositions of electrodes and electrolytes were found to undergo varying degree of degradation due to chromium poisoning [31, 34, 35]. The approaches used in anode-supported SOFCs to suppress Cr poisoning inform

4

our efforts to suppress Cr migration from the cathode metal support in this work.

With implementation of aforementioned strategies to suppress Cr poisoning, stack lifetime in anode supported cells [10] and ferritic steel substrate supported SOFCs [29] have been demonstrated. For instance, Topsoe Fuel Cells demonstrated anode supported stack operation with coated FeCr-based interconnects that generated power for 13,000h with minimal degradation [10, 36], and Ceres Power demonstrated operation up to 6,400h with 0.3-0.45% khr^{-1} degradation in ferritic steel substrate supported SOFCs [29]. However, in both demonstrations the power density is substantially low, and not compatible with vehicular applications.

In this work, the performance vs. durability tradeoff is studied across a range of operation temperatures and catalyst compositions in high-performance MS-SOFCs. The major degradation mechanisms are isolated and addressed individually. Significant improvement in MS-SOFC durability is achieved by implementing preoxidation of the metal support, atomic layer deposition (ALD) protective coatings, and *in situ* catalyst pre-coarsening. Combining these additional steps into the MS-SOFC fabrication process leads to two orders of magnitude decrease in degradation rate while preserving high performance.

Experimental

2.1 Cell fabrication

Green cells were assembled by laminating individual 10Sc1CeSZ (DKKK, Japan) electrode backbone and electrolyte, and stainless steel (P434L alloy, water atomized, Ametek Specialty Metal Products) support layers prepared by tape-casting with aqueous tape-casting binder. The electrode and support layers were prepared with polymethyl methacrylate poreformer beads (Esprix Technologies). The resulting symmetric-structure MS-SOFCs were laser-cut (Hobby model, Full Spectrum Laser) from the laminated tape-cast layers and the edges were cleaned with an air duster to remove any loose particles. Cells were then debinded in a box furnace by firing in air at 525 °C for 1h with 0.5 °C min^{-1} heating rate to slowly remove the binder and pore former. The cells were then sintered at 1350 °C for 2h in a tubular furnace while flowing 2% hydrogen/argon. The resulting cells were 30 mm in diameter which had 250 μm thick porous metal supports, 25 μm thick porous cathode and anode backbones, and 12 μm thick 10Sc1CeSZ electrolyte. More details about optimization of each cell layer can be found in our previous work [12].

2.2 Catalyst precursors and cell infiltration

Precursor mixtures of metal nitrates (Sigma Aldrich) were prepared with the intended final stoichiometric composition. A surfactant, Triton-X 100 (Sigma Aldrich) with loading of 0.3 g per 2 g of resulting catalyst was added to metal

6

nitrates and dissolved in 20 to 100 wt% (vs. catalyst) of water. More detailed description can be found in our previous report [12]. The areas of MS-SOFCs that were not intended to be infiltrated were covered with acrylic paint mask (Liquitex) providing 1 cm^2 active area. The cells were then fired at 3 °C min^{-1} heating rate to 600 °C or 850 °C for 30 min in air to convert the precursors to the intended oxide phases [12]. The cells were re-infiltrated a number of times: (1) cathodes were infiltrated a total of three times, with firing at 850 °C, 600 °C, and 600 °C (2) while anodes were infiltrated three to four times, with firing at 850 °C, 600 °C, 600 °C, and 600 °C. In the case of composite cathodes (see section 2.3), up to five infiltrations were implemented. For instance, a ternary composite cathode has three different layers [25], an electronic conductor that provides good electronic conduction at the triple phase boundary (TPB) and was infiltrated first and sintered at 850 °C, an ionic conductor that provides good ionic conduction and was infiltrated second and sintered at either 600 °C or 850 °C, and the bulk catalyst for the oxygen reduction reaction (ORR) which was infiltrated three times and sintered at 600 °C. XRD measurements on catalyst powders were obtained using a Bruker D2 Phaser powder diffractometer.

2.3 Cathode and anode candidates

Five categories of cathode catalysts were screened in full cells, including: (1) perovskites: $La_{0.85}Sr_{0.15}MnO_{3-\delta}$ (LSM), $La_{0.8}Sr_{0.2}FeO_{3-\delta}$ (LSF), $LaNi_{0.6}Fe_{0.4}O_{3-\delta}$ (LNF), $(La_{0.60}Sr_{0.40})_{0.95}Co_{0.20}Fe_{0.80}O_{3-\delta}$ (LSCF), $La_{0.6}Sr_{0.4}CoO_{3-\delta}$ (LSC), $Sm_{0.5}Sr_{0.5}CoO_{3-\delta}$

(SSC); (2) nickelates: $Pr_2NiO_{4+\delta}$ (PNO), $La_2NiO_{4+\delta}$ (LNO), $Nd_2NiO_{4+\delta}$ (NNO); (3) praseodymium oxide (PrO_x); (4) binary composites: $La_{0.85}Sr_{0.15}MnO_{3-\delta}$-$Sm_{0.20}Ce_{0.80}O_{2-\delta}$ (LSM-SDC), Pr_6O_{11}-$Sm_{0.20}Ce_{0.80}O_{2-\delta}$ (PrO_x-SDC), $Sm_{0.5}Sr_{0.5}CoO_{3-\delta}$-$Sm_{0.20}Ce_{0.80}O_{2-\delta}$ (SSC-SDC); and (5) ternary composites: $La_{0.85}Sr_{0.15}MnO_{3-\delta}$ -$Sm_{0.20}Ce_{0.80}O_{2-\delta}$ -Pr_6O_{11} (LSM-SDC-PrO_x), and $Sm_{0.5}Sr_{0.5}CoO_{3-\delta}$-$Sm_{0.20}Ce_{0.80}O_{2-\delta}$-$Pr_6O_{11}$ (SSC-SDC-PrO_x). Anode catalysts included different Ni concentration mixed with $Sm_{0.20}Ce_{0.80}O_{2-\delta}$ (SDC). The Ni fraction varied from 10-50 vol%.

2.4 Preoxidation and ALD coating

Some MS-SOFCs were preoxidized in air at 850 °C for 10 h, as indicated in the text. ALD coating was implemented using an Oxford FlexAL (for CoO_x and Al_2O_3) and an ICOT system (for CeO_2 and Y_2O_3) on either cathode or anode side of MS-SOFCs. The cells were placed on a Si wafer and the edges of cells were covered with Kapton tape (for CoO_x and Al_2O_3) or Al foil (for CeO_2 and Y_2O_3) ensuring only the top side of cells gets coated. Cathode side was coated with CoO_x, Y_2O_3, or Al_2O_3, while anode was coated with CeO_2. Bis(cyclopentadienyl)cobalt(II), tris(methylcyclopentadienyl)yttrium(III), tris(dimethylamido)aluminum(III), tris(i-propylcyclo-pentadienyl)cerium(III) were used as the organometallic precursors for CoO_x, Y_2O_3, Al_2O_3, and CeO_2 respectively, and deionized water was used as the oxygen source. Both CoO_x and Al_2O_3 were coated between 40-80 °C (chamber and stage temperature) with average of 0.6 Å/cycle until a desired coating thickness was achieved. The chamber temperature for CeO_2 and Y_2O_3 were 250 °C with expected

growth rate of ~1.0 Å/cycle; 15 and 20 cycles were performed for CeO_2 and Y_2O_3, respectively. The coatings were too thin to study via SEM, but the calibration for each coating recipe was conducted on a Si wafer and the thickness was measured via ellipsometry. The catalyst infiltration and calcination immediately followed.

2.5 Cell testing

Complete cells were mounted on 410 stainless steel rigs using GM31107 glass paste (Schott, Germany). Each side of the cell was spot-welded with a small Pt mesh on two NiCr wires, for good electrical contact. The applied glass paste was heated to 200 °C at 2 °C min^{-1} and then heated to 700 °C at 10 °C min^{-1} and held for one hour. The anode chamber was then flushed with nitrogen followed by hydrogen humidified at room temperature. The cathode side was exposed to static air. The i-V and electrochemical impedance spectroscopy (EIS) measurements were recorded with a VMP3 multichannel potentiostat and current booster (Biologic).

Results and Discussion

3.1 Durability of cathode and anode candidates

Catalyst performance and durability screening was performed on YSZ-based MS-SOFCs with 12 μm YSZ electrolyte thickness [25], **Table 1**. The cathode compositions tested in cathode/YSZ/$SDCN_{20}$ MS-SOFC cell configuration include five families: (1) perovskite cathodes, (2) nickelate cathodes, (3)

praseodymium oxide, (4) binary layered composites, and (5) ternary layer composites. The initial OCV was 1.12 ± 0.03 V (theoretical value is 1.12 in 3% humidified hydrogen), and remained within 2% of the initial value after 100 h of operation at 700 °C and 0.7 V. The overall peak power density and degradation at 700 °C are grouped by cathode family in **Table 1**.

Perovskites show the lowest overall peak power density and highest degradation, followed by nickelates which exhibit lower degradation. Pr_6O_{11} (PrO_x) stands out as having the highest peak

power density (1.3 W cm^{-2}) but shows similar degradation to perovskites. Although the intrinsic transport properties of nano-scale ceramics remain to be investigated, the high peak power density in cells with PrO_x cathode was attributed to enhanced oxygen ion transport properties [25]. The peak power density and degradation for different cathode catalysts are summarized in **Table 1 and Fig 1a**. The binary composite cathodes exhibit the highest overall peak power density and the lowest degradation rates, **Fig. 1a**. Due to severity of degradation for each cathode composition, PrO_x was chosen solely due to its higher initial performance. However, we do intend to revisit composite cathodes in the future with new fabrication enhancements [25].

Table 1. MS-SOFC performance and stability at 0.7 V with various cathode and anode catalyst compositions at 700 °C.

| Abbreviation	OCV (V)	Peak Power (W/cm^2)	% Degradation / 100 h
Perovskites			
LSM	1.12	0.9	16
SSC	1.10	1.0	27
LSC	1.09	1.0	29
LSF	1.09	0.7	30
LNF	1.11	0.7	33
LSCF	1.10	0.8	44
Nickelates			
NNO	1.11	1.0	13
LNO	1.10	1.0	14
PNO	1.09	0.6	20
Pr_6O_{11}			
Pr_6O_{11}	1.12	1.3	28
Binary Composites			
LSM-SDC$_{600}$*	1.09	1.1	14
LSM-SDC$_{850}$**	1.12	1.1	15
PrO$_x$-SDC	1.10	1.2	17
SSC-SDC	1.11	1.1	18
Ternary Composites			
LSM-SDC-PrO$_x$	1.12	1.1	19
SSC-SDC-PrO$_x$	1.09	1.1	22
Anodes			
10%Ni-SDC	1.11	1.28	44
20%Ni-SDC	1.10	1.30	43
30%Ni-SDC	1.12	1.32	40
40%Ni-SDC	1.12	1.34	43
50%Ni-SDC	1.11	1.35	40

*SDC calcined at 600 °C; **SDC calcined at 850 °C

Performance degraded substantially during the initial 100 h of operation for all families of cathodes. For instance, the cell with PrO$_x$ cathode and SDCN$_{20}$ (20 vol% Ni- 80vol% SDC) anode degrades ~30%/100 h, **Fig. 1b**. A separate batch of PrO$_x$/YSZ/SDCN MS-SOFCs was used to isolate the anode contribution to performance degradation by varying the Ni:SDC ratio of the

infiltrated catalyst from 10 to 50 vol%. Peak power increases moderately with Ni concentration, while the degradation rates remained similar, **Table 1**. This suggests that degradation is dominated by the cathode catalysts. In our preceding work [25], $SDCN_{40}$ (40 vol% Ni-SDC) was selected for high performing cells based on the balance between R_{ohm} and R_{pol} values, while Ni ratio above 40 vol% in the anode lead to marginal increase in power but rapid degradation [25]. $SDCN_{40}$ remains the anode of choice for further durability studies in this work.
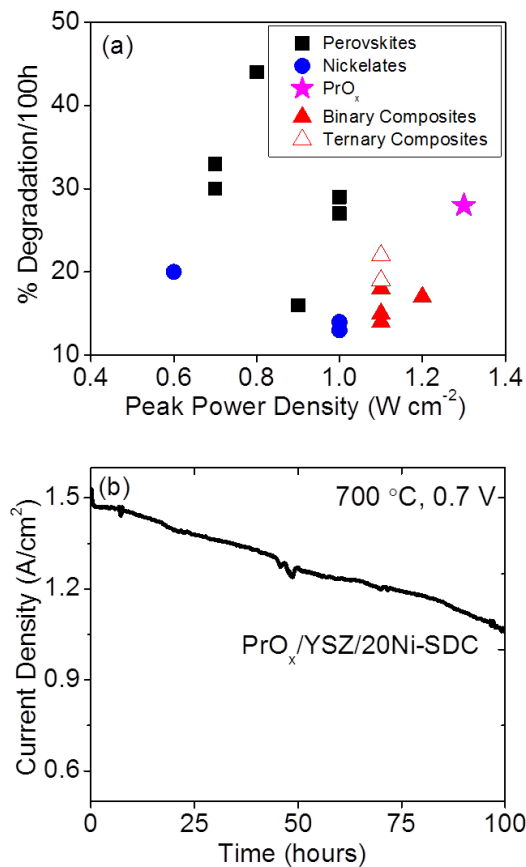

Figure 1. Cathode screening. (a) Degradation and fuel cell performance with various cathode catalysts. (b) Baseline MS-SOFCs degradation at 700 °C and 0.7 V for selected PrO_x cathode catalyst.

3.2 Microstructure and phase stability

It is well known that SOFC nanocatalysts tend to coarsen at elevated temperatures and/or during electrochemical operation, which leads to decline in active surface area of the catalyst and consequently performance degradation. Microstructural changes (e.g. coarsening) occur to minimize the local surface energy through particle rearrangement and evolution of grain boundaries [37]. Our previous long-term durability tests on LSM/YSZ/SDCN$_{20}$ cells revealed rapid performance degradation (70%/1,000 h) which was linked to catalyst coarsening and chromium poisoning of the LSM catalyst [16]. Such magnitude of degradation does not meet the requirements for vehicular applications.

In this work, an attempt is made to separate the impact of thermal coarsening and chromium poisoning in MS-SOFCs. SEM analysis was performed on cathode and anode nanocatalysts in PrO$_x$/YSZ/SDCN$_{40}$ cells at 0th hour (heated to 700 ºC and immediately cooled) and after *in situ* thermal annealing (700 °C, 100 h) and electrochemical operation (700 °C, 0.7 V, 100 h). A fluffy and porous PrO$_x$ microstructure (at 0th hour) transforms to a dense PrO$_x$ blanket during operation. The catalyst coarsening seems to be predominantly thermally driven, while additional impact of electrochemical operation is not as evident after the initial 100 h, **Fig. 2a**. The microstructure of anode catalyst remains visibly stable during operation, **Fig. 2b**. These observations suggest that cathode coarsening is a dominant degradation

mode of MS-SOFCs. Due to presence of stainless steel metal supports, MS-SOFCs are also known to undergo Cr poisoning of the cathode catalyst [2, 13-15], which will be addressed in more detail in Section 3.4.
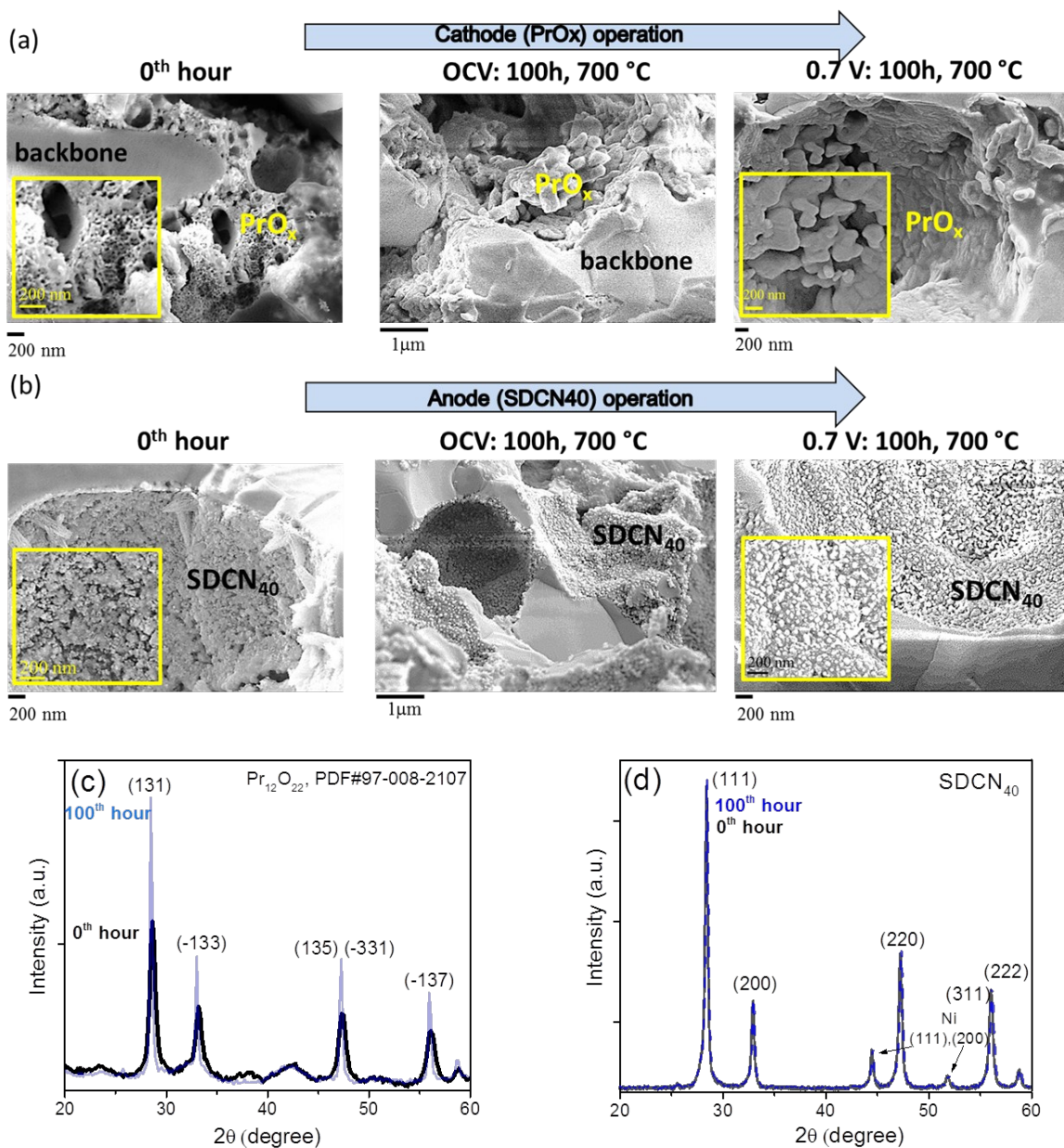
Figure 2. Nanocatalyst structure and phase stability. (a) Cathode (PrOx) and (b) anode (SDCN$_{40}$) catalyst coarsening via thermal annealing at 700 °C and

continuous electrochemical operation at 0.7 V for 100 h. (c) Powder X-ray diffraction on PrO_x cathode catalyst calcined at 600 °C (black) and after thermal annealing at 700 °C (blue) in air for 100h h. (d) X-ray diffraction patterns for of $SDCN_{40}$ anode catalyst upon reduction at 700 °C for 1 hour (black), and after 100 h of thermal annealing at 700 °C in 3% humidified hydrogen (blue).

Despite the microstructural evolution, the PrO_x remains in the intended phase. XRD of PrO_x catalyst powder showed stable monoclinic Pr_6O_{11} phase after 100 h of thermal annealing at 700 °C, **Fig. 2c**. The ratio of peak intensities remained consistent after thermal annealing, indicating homogeneous bulk PrO_x. The signature reflections show decreased peak broadening, consistent with the catalyst coarsening observed with SEM. $SDCN_{40}$ catalyst powder was thermally annealed in 3% humidified hydrogen for 100 h at 700 °C. XRD patterns show mainly SDC phase and the major Ni signature peaks, **Fig. 2d**. The peak width and peak ratio remained unchanged, indicating retained $SDCN_{40}$ phase and minimal coarsening.
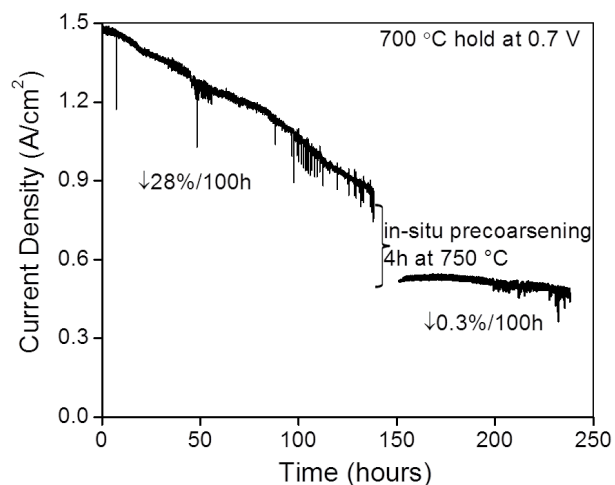
3.3 Catalyst pre-coarsening

Rapid thermal coarsening of PrO_x nanocatalyst in MS-SOFCs presents a major durability challenge. We propose to address this by pre-coarsening the catalyst *in situ* at elevated temperature, to rapidly achieve the stable, coarsened microstructure expected after prolonged electrochemical operation. To demonstrate, a $PrO_x/SCSZ/SDCN_{40}$ cell operated for 140 h at

700 °C and 0.7 V was then pre-coarsened *in situ* at OCV for 4h at 750 °C. After pre-coarsening, substantial improvement in degradation to 0.3%/100 h was achieved, **Fig. 3**. Although the catalyst pre-coarsening leads to ~50% decrease in performance, the two order of magnitude improvement in durability is encouraging.

Based on this dramatic effect of intentional *in situ* thermal coarsening, we explored a range of coarsening temperatures to optimize the tradeoff between performance and stability observed above. A wide operating temperature range between 600 – 750 °C was considered to elucidate the pre-coarsening approach, and cells were pre-coarsened between 25 and 100°C above the operating temperature at the beginning of life, **Table 2**. Due to the glass sealing procedure all cells had to be briefly heated to 700 °C, which allowed for initial comparison. Initial peak power for the entire batch of cells used in the matrix varied less than 5% and OCV was 1.12 ± 0.02 V at 700 °C in 3% humidified hydrogen.

Figure 3. Impact of *in situ* catalyst pre-coarsening. MS-SOFC durability at 700 °C and 0.7 V before and after *in situ* catalyst pre-coasening at 750°C for 4 h.

Table 2. Pre-coarsening vs. operating temperature matrix for $PrO_x/SCSZ/SDCN_{40}$ cells.

Baseline cells (without pre-coarsening) were used for durability comparison and show substantially larger degradation than pre-coarsened cells, **Fig 4**.

Baseline

Operation temperature (°C)	*In situ* pre-coarsening temperature for 4 h (°C)			
750				800
700		725	750	800
650		700	750	
600	650	700		

degradation is the lowest at 700 °C and increases in both temperature directions. Higher operating temperature may lead to rapid catalyst coarsening and accelerated Cr poisoning of the cathode catalyst [2, 13-15],

while the lower operating temperature may lead to increased sensitivity of the performance to catalyst evolution, and breakaway oxidation of the metal support (~600 °C) [2, 3], which will be addressed in more detail below in this section. Durability of selected cells at different temperatures is summarized in **Fig. 4b**. With *in situ* pre-coarsening the degradation is significantly reduced at all operating temperatures. Larger temperature difference between pre-coarsening and operation leads to enhanced durability, with the exception of 600 °C operation. For instance, a cell operated at 700 °C was pre-coarsened at 725, 750, and 800 °C. Pre-coarsening at 725 °C leads to 3x lower degradation and the smallest performance tradeoff, 25% drop in power density. A cell pre-coarsened at 750 °C shows 45% decrease in power density and 3.9%/100 h degradation, which is an order of magnitude improvement over a baseline cell. Pre-coarsening at 800 °C leads to 0.3%/100 h degradation at 700 °C and 52% decrease in power density. Similarly, a cell pre-coarsened at 750 °C and operated at 650 °C shows zero degradation during 100 h and 73% decrease in power density, **Fig. 4a**.

Despite the expectation that catalyst microstructure evolves more slowly at lower temperature, rapid degradation is observed at 600 °C, suggesting a different dominant degradation mechanism, **Fig 4a-b**. The corrosion stability of stainless steel greatly depends on the formation of a continuous chromium oxide layer on the surface which limits the rate of oxidation by acting as a

diffusion barrier for oxygen [38]. Although the oxidation rate of metals generally decreases
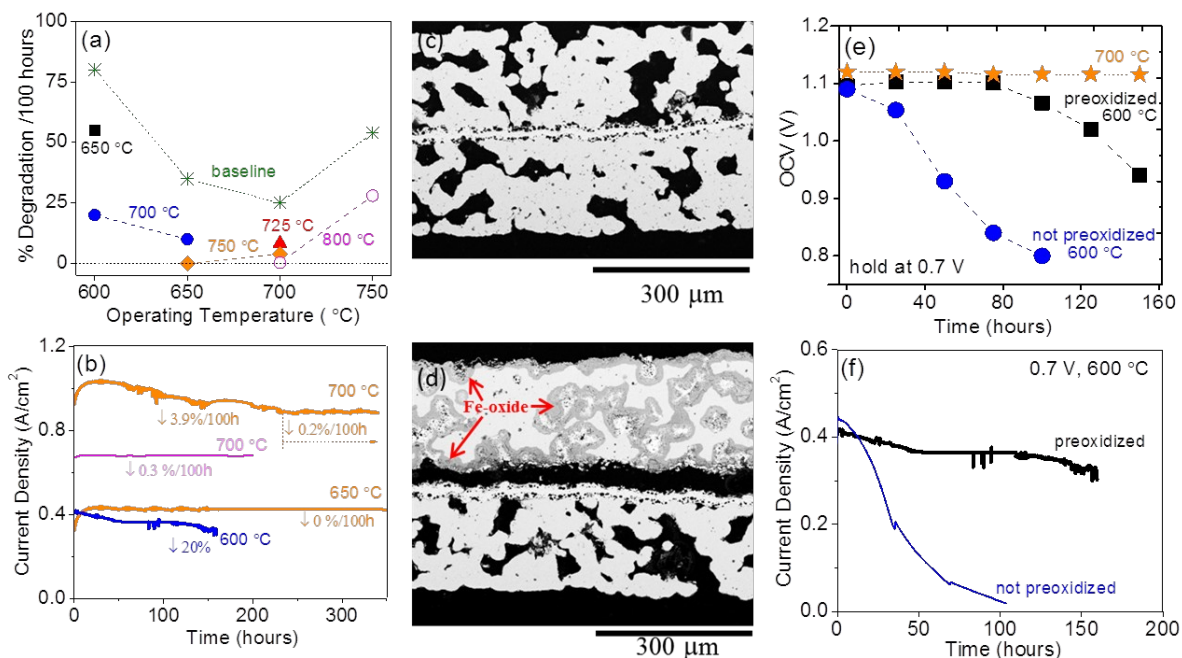
Figure 4. Impact of pre-coarsening and preoxidation treatment. (a) Degradation rate at various operating temperatures for cells pre-coarsened at the temperatures indicated in the figure (text and color). (b) Continuous operation at various temperatures (labeled in the figure) with catalyst pre-coarsening at various temperatures indicated by the color scheme in (a). Cross sectional SEM images of symmetric cell architecture (top is air side) after 100 h and 0.7 V operation at (c) 700 °C and (d) 600 °C. (e) OCV stability at 700 °C and 600 °C. (f) Continuous operation at 600 °C with and without preoxidation of the metal support.

at lower temperatures, several studies of FeCr alloys indicated that the oxidation rate increases dramatically at certain lower temperature intervals where formation of a continuous chromia layer does not occur [39-41]. This phenomenon is known as breakaway oxidation, and occurs when Cr diffusion to the metal/oxide interface is slower than consumption of chromium by oxidation [38, 42]. Hence, a continuous and protective chromia oxide scale on the surface of the metal is not formed and rapid iron oxidation prevails [38, 42]. With MS-SOFCs, the stainless steel support (P434 alloy) appears to undergo breakaway oxidation at 600 ºC, which was evident by the air-side metal support being weakened to the point that it delaminates from the ceramics when removing the cell from the test rig. A full cell operated at 700 ºC for 350 h does not show any Fe oxide (Fe_2O_3) formation in the metal support, while the cell operated at 600 ºC shows severe breakaway oxidation through the entire bulk of the air-side metal support, **Fig 4c-d**. Breakaway oxidation is also associated with a rapid OCV drop, which is consistent with performance degradation, **Fig. 4e-f**. We suspect that the OCV drop arises from cracks in the ceramic layers due to mechanical stress associated with volume expansion of the metal support during breakaway oxidation.

To address the breakaway oxidation, cells were preoxidized in air at 850 ºC for 10 h before catalyst infiltration into the cell. This fabrication step allows for formation of continuous chromia oxide scale on the metal supports and

20

can potentially suppress the Fe oxidation. Indeed, preoxidation leads to improved durability at 600 ºC when compared to non-preoxidized cells, **Fig. 4f**. Although the preoxidation step prolongs the cell operation beyond 100 h at 600 ºC, the air-side metal support weakens and OCV eventually undergoes a rapid drop, **Fig. 4e**. Therefore, operation between 650-700 ºC is desirable for MS-SOFCs. Future efforts to eliminate breakaway oxidation are also warranted.
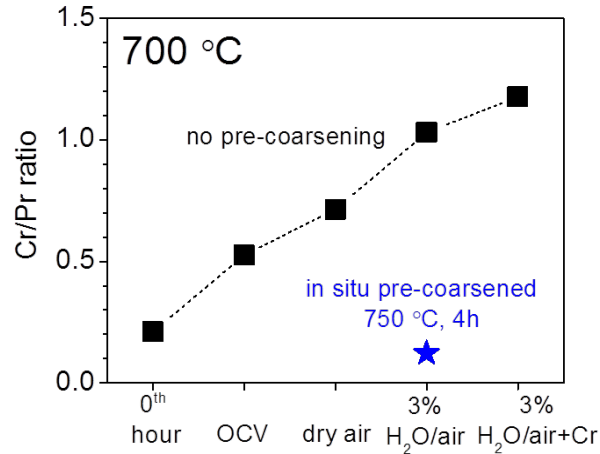
3.4 Chromium poisoning

Chromium poisoning is considered as a second major degradation mechanism in MS-SOFCs [16]. Although overshadowed by substantial catalyst coarsening, this degradation mechanism becomes more pronounced during extended electrochemical operation [16] and warrants further study. In the present symmetric architecture, the stainless steel support is a high-surface-area Cr source in close proximity to the cathode active sites. This is expected to be more problematic than the dense stainless steel interconnects used in conventional stacks of ceramic cells.

Multiple PrO_x/SCSZ/$SDCN_{40}$ cells were operated at 700 °C for 100 h under different air moisture content. Two baseline cells were used for comparison; a cell at 0th hour of operation (heated to 700 °C and immediately cooled), and a cell held at OCV at 700 °C for 100 h. Performance degradation was accelerated by 22% in dry air and 30% in humidified air after 100 h at 0.7 V,

which further indicates that PrO_x coarsening is a major degradation mechanism in MS-SOFCs but the additional 8% degradation with humidified air can be attributed to promoted Cr poisoning. EDS analysis was conducted on the cells to quantify Cr content in the porous cathode ceramic layer. The selected region of interest was deep within the porous structure of a cell, near the electrolyte/cathode interface. When switching from dry to 3% humidified air, the Cr/Pr ratio is increased by 43%, **Fig. 5**. EDS results reveal saturation of Cr:Pr ratio at 1:1, possibly indicating formation of a stable $PrCrO_x$ phase. To verify, a separate cell with additional infiltration of Cr nitrate on top of PrO_x was also tested. After 100 h of operation at 0.7 V and 700 °C, the Cr/Pr ratio was ~1:1, confirming the formation of $PrCrO_x$ phase, **Fig. 5**.

The impact of *in situ* pre-coarsening on Cr poisoning of PrO_x was also investigated. A pre-coarsened cell was operated at 700 °C for 100 h in 3% humidified air. The post-operation EDS analysis showed suppressed Cr poisoning in the cell, **Fig. 5**. This could be attributed to substantial catalyst coarsening and reduced catalyst surface area for Cr poisoning, or densification of the catalyst coating on the metal support blocking Cr evaporation. The *in situ* pre-coarsening seems to conveniently suppress both catalyst coarsening and Cr poisoning degradation mechanisms.

Figure 5. Impact of chromium poisoning. Cr/Pr ratio from EDS spectra near the catalyst/backbone interface for a cell at 0th hour, cell held at OCV for 100 h, and cells operated at 700 °C for 100 h in different air environments.
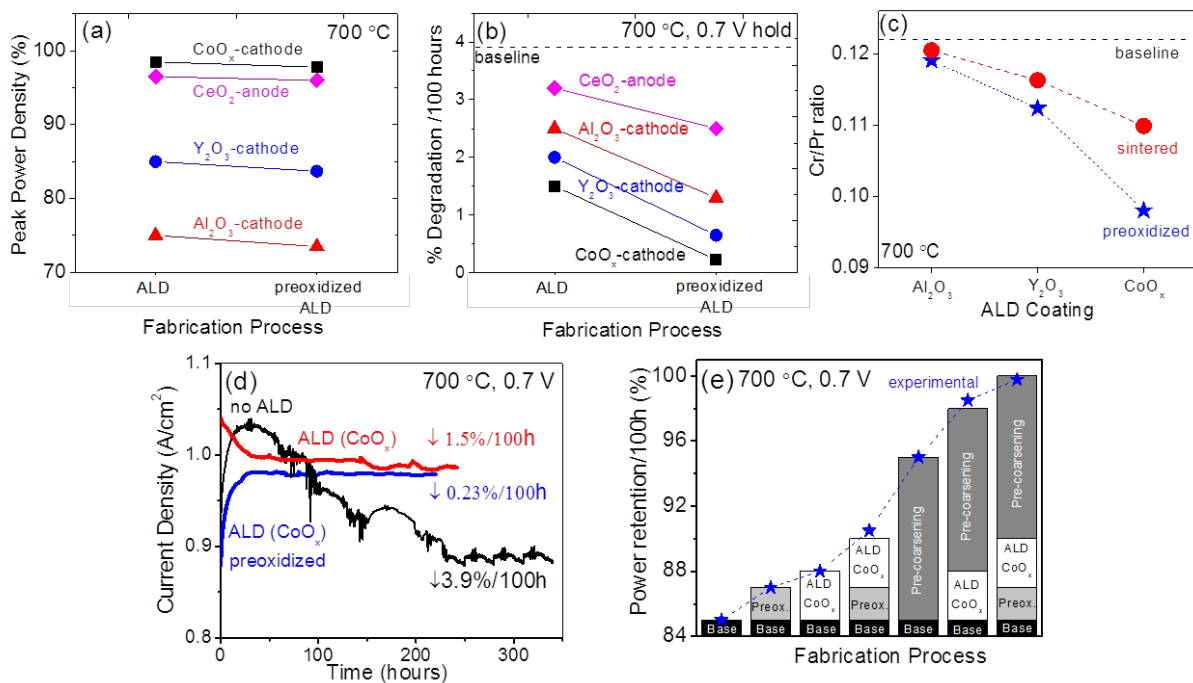
3.5 ALD protective coatings

Atomic layer deposition (ALD) technique is highly advantageous over other deposition techniques in its capability to provide conformal and uniform coatings at true nanoscale, even deep within a porous structure [43-44]. Such coatings have proved to be effective in suppressing microstructural coarsening [45] and/or Cr migration [46] and boosting electrochemical surface kinetics in SOFCs [47]. Our early efforts for anode-Ce ALD implementation were sparked by an attempt to reduce agglomeration of the fine Ni catalyst particles during long-term electrochemical operation. In the preceding sections of this work however, it has been shown that anode has minimal impact on MS-SOFC degradation, which is dominated by PrO_x coarsening and Cr poisoning. Therefore, a variety of protective coatings were implemented in this work to further suppress Cr migration.

23

On the air side, coatings were applied to sintered cell before catalyst infiltration, so as to provide a conformal Cr-blocking coating on the stainless steel. The air-side metal support was coated with CoO_x, Y_2O_3 or Al_2O_3. The fuel-side metal support and electrode were coated with CeO_2 after $SDCN_{40}$ infiltration to stabilize the $SDCN_{40}$ microstructure. Coatings were implemented on as-sintered and preoxidized cells for comparison. Cells with 20 nm CoO_x coating and preoxidation provide minimal loss in initial power density, while ~2 nm Y_2O_3 or Al_2O_3 led to significant loss in power density, which can be attributed to their insulating properties. A 2 nm CeO_2 coating leads to marginal (3-4%) decrease in power density, **Fig. 6a**.

Durability of the MS-SOFCs was greatly enhanced by the ALD coatings. To minimize the impact of catalyst coarsening on degradation, all cells were *in situ* pre-coarsened (750 ºC, 4h) before durability studies. The cells with ALD-CoO_x coating show remarkably improved degradation rate during 100 h of operation at 700 ºC and 0.7 V. An order of magnitude improvement in degradation rate (1.5%/100 h) was measured for cells coated directly after sintering, and two orders of magnitude improvement (0.23%/100 h) for cells preoxidized before ALD coating. The thin cathode-side ALD coating is implemented into MS-SOFC before catalyst infiltration and firing. During catalyst firing in air the chromia scale (Cr_2O_3) tends to form on the stainless steel surface, which may crack the thin ALD coating, allowing more Cr migration from the stainless steel support. On the other hand, preoxidized

cells already have a thin chromia scale (~1 μm) that does not tend to grow further at a high rate. Therefore, the integrity of the ALD-CoO_x coating is most likely preserved during catalyst infiltration and operation for pre-oxidized cells. Hence, the preoxidized cells show superior durability, **Fig. 6b**. Other coatings including Y_2O_3 and Al_2O_3 also lead to improvements in durability; however, due to significant performance tradeoff the CoO_x protective coating was selected as the major candidate to suppress Cr poisoning in MS-SOFCs with minimal impact on performance. CeO_2 coating on the anode does not lead to significant durability improvements, which further points to Cr poisoning on the air side as the second major degradation mechanism in MS-SOFCs, **Fig 6a-b**.

Figure 6. Impact of preoxidation and ALD protective coatings. (a) Normalized initial performance and (b) degradation rate for as-sintered and

pre-oxidized cells with various coatings. (c) EDS results from cells operated at 0.7 V and 700 ºC for 200 h with ALD coatings on as-sintered or preoxidized air-side metal support. Pre-coarsened cell without coatings is used as a baseline. (d) Continuous operation of pre-coarsened cells with no additional treatment (black), ALD-CoO$_x$ coating (red), and preoxidation followed by ALD-CoO$_x$ coating (blue). (e) Bars represent quantified power retention (percentage of remaining power density after 100 h of operation vs. beginning of life) observed for the post-sintering fabrication processes, individually and combined. Each process is associated with different color and marking. Experimental results from full cells are overlaid (blue stars).

Indeed, post-operation EDS analysis on pre-coarsened cells with ALD coatings shows suppressed Cr concentration, **Fig. 6c**. Preoxidizing before ALD-CoO$_x$ coating provides 25% reduction in Cr concentration; ALD-CoO$_x$ alone provides 10% reduction. Addition of the preoxidation step suppressed Cr poisoning for all three cathode coatings.

Long-term electrochemical operation (220-350 h) was conducted on MS-SOFCs with and without ALD-CoO$_x$ coating. Degradation of 2.3% kh^{-1} was measured for a preoxidized and ALD-CoO$_x$ coated cell, compatible with the ~10,000 h desired lifetime of MS-SOFCs for vehicular applications, **Fig. 6**d. The major three MS-SOFC post-sintering fabrication processes found here to be crucial in stabilizing the performance of MS-SOFCs, in the respective order, include: (1) preoxidation of the metal support which leads to formation

of protective and conductive chromia scale, (2) ALD coating of CoO which suppresses Cr migration from the metal support, and (3) *in situ* catalyst pre-coarsening which significantly enhances electrochemical durability by accelerating particle coarsening and reducing the active surface area for chromium poisoning.

To further isolate the impact of each post-sintering fabrication process on MS-SOFC durability, a series of cells with single or multiple post-sintering processing steps was prepared. A set of two cells were tested for each fabrication condition. A baseline set contained catalyst that was not pre-coarsened and had no additional processing before operation. A second set contained preoxidized metal support as an additional process. A third set contained ALD-CoO$_x$ coating as an additional process. A fourth set contained *in situ* pre-coarsened catalyst as an additional process. Finally, a combination of two or more processes was implemented in a single cell. Systematic analysis suggests that fabrication processes are additive towards durability improvements of MS-SOFCs, corresponding to approximate agreement between stacked bars for each individual process and overlaid experimental results, **Fig 6e**. The impact of pre-coarsening on power retention is dominant, followed by the ALD-CoO$_x$ and preoxidation, respectively.

3.6 Progress in MS-SOFC durability

Our preceding performance efforts [25] showed substantial improvements in MS-SOFC peak power density (performance was doubled) by introducing new catalyst compositions, more conductive ceramics, and thinner electrolyte. In this work, we focused on durability aspect of MS-SOFCs. Aggregating the improvements identified in sections 3.3-3.5 including preoxidation of the metal support, protective ALD-CoO_x coating, and *in situ* catalyst pre-coarsening resulted in two orders of magnitude improvement in power retention of MS-SOFCs, **Fig. 7a**. Performance degradation of 2.3% khr^{-1} was achieved at 700 ºC and 0.7 V, **Fig. 7b**.

The respective EIS curves at 0th hour and at the last hour of electrochemical operation show increase in R_{ohm} and R_{pol} for a baseline non-pre-coarsened cell, while a cell with all three processing improvements shows relatively stable EIS, **Fig. 7c**. The increase in R_{ohm} and R_{pol} during operation is dominated by the cathode catalyst pre-coarsening (similar occurs with *in situ* pre-coarsening), as shown by the cross-sectional SEM images of baseline and *in situ* pre-coarsened cells. PrO_x coarsening is evident in the baseline cell during electrochemical operation, **Fig 2a**, while the *in situ* pre-coarsened catalyst does not seem to coarsen further even after 200 h of electrochemical operation, **Fig. 7d-f**.
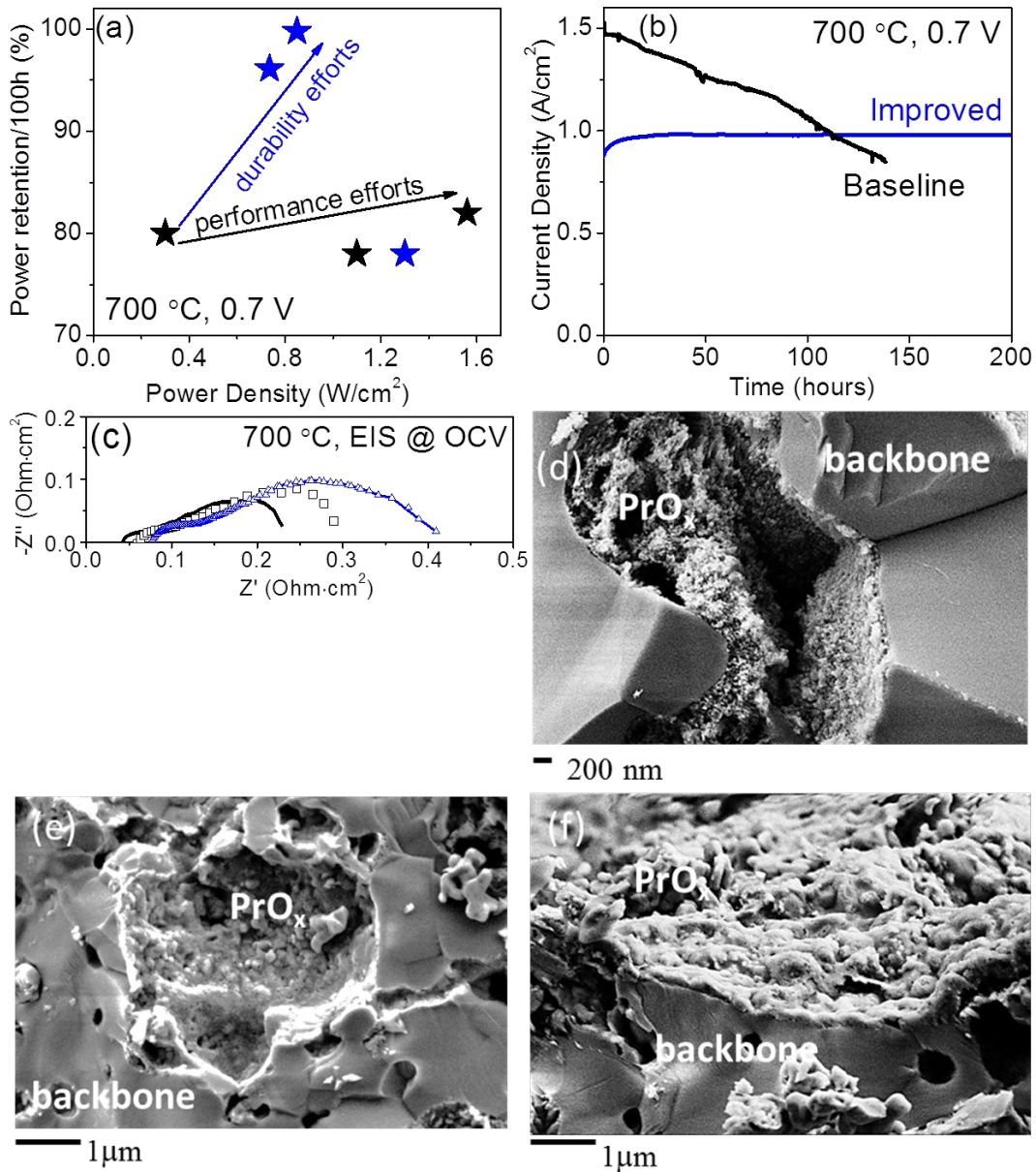
Figure 7. Durability progress. (a) Peak power density and power retention with various cell improvements. (b) Long-term durability for baseline and improved cell at 700 °C and 0.7 V. (c) Corresponding EIS spectra at OCV and 700 °C for baseline cell [black: 0th hour (line), 100th hour (squares)] and improved cell [blue: 0th hour (line) and 200th hour (triangles), the two data

sets overlap]. Cross section SEM images of (d) fresh PrO_x, (e) after *in situ* pre-coarsening, and (f) after 200 h at 0.7 V and 700 °C.

Preoxidation of the metal support and application of a thin ALD-CoO_x coating do not seem to inhibit conduction or catalytic properties of the cell, as shown by unaffected peak power density, **Fig. 6a**. While enhancing the MS-SOFC durability, a significant performance tradeoff was made. A 35% loss in initial power density was measured; however, two orders of magnitude improvement in degradation rate is encouraging, **Fig. 7a-b**. Since durability studies in this work were conducted on cells with thick SCSZ electrolyte (12 μm), an additional ~20% increase in overall power density could be expected with thin SCSZ electrolyte (7 μm), based on the previous performance efforts [25].

Conclusions

Motivated by the requirements for use in vehicle range extenders, symmetric-architecture MS-SOFCs have been optimized for high performance and longevity. Previously, we have demonstrated high power density (1.56 W cm^{-2} at 700 ºC) for stainless steel MS-SOFCs using Pr_6O_{11} cathode, $SDCN_{40}$ anode, and optimized cell configuration. In this work, we have explored the tradeoff between performance and durability and identified the major degradation mechanisms: cathode catalyst coarsening and Cr poisoning. The impact of anode on MS-SOFC degradation was found to be minimal in comparison to the cathode contribution.

Preoxidation of the metal support was found to be beneficial for the longevity of MS-SOFCs, leading to formation of conductive chromia scale. To prevent Cr migration from the metal support and chromia scale to the catalyst sites, a thin CoO_x ALD coating (20 nm) was implemented on air-side metal support after preoxidation. Both fabrication steps only marginally impacted the cell ASR. The catalyst coarsening was accelerated via an *in situ* pre-coarsening step at the beginning of cell life (OCV, 750 ºC, 4 h), which stabilized the catalyst microstructure during long-term electrochemical operation. The EIS and SEM results confirmed that cathode coarsening dominates the cell ASR during prolonged operation. With combination of these fabrication steps, the degradation rate of MS-SOFCs has been improved by two orders of magnitude at 0.7 V and 700 ºC, to 2.3%/kh, which is within the target range for vehicular applications. A 35% loss in initial power density was measured after MS-SOFC preoxidation, ALD coating, and pre-coarsening, which is a reasonable tradeoff considering the dramatic durability improvement.

Technical Center North America for providing cost share and helpful discussion.

The views and opinions of the authors expressed herein do not necessarily state or reflect those of the United States Government or any agency thereof. Neither the United States Government nor any agency thereof, nor any of their employees, makes any warranty, expressed or implied, or assumes any legal liability or responsibility for the accuracy, completeness, or usefulness of any information, apparatus, product, or process disclosed, or represents that its use would not infringe privately owned rights.

References

[1] M. C. Tucker, G. Y. Lau, C. P. Jacobson, L. C. DeJonghe, S. J. Visco, ECS Transactions, 7 (2007) 279-284.
[2] M.C. Tucker, Journal of Power Sources, 195 (2010) 4570-4582.
[3] M.C. Tucker, G. Y. Lau, C. P. Jacobson, L. C. DeJonghe, S. J. Visco, Journal of Power Sources, 171 (2007) 477-482.
[4] Y. B. Matus, L. C. De Jonghe, C. P. Jacobson, S. J. Visco, Solid State Ionics, 176 (2005) 443-449.
[5] M. C. Tucker, International Journal of Hydrogen Energy, 43 (2018) 8991-8998.
[6] M. C. Tucker, Journal of Power Sources, 395 (2018) 314-317.
[7] M. C. Tucker, G. Y. Lau, C. P. Jacobson, L. C. DeJonghe, S. J. Visco, Journal of Power Sources, 175 (2008) 447-451.

[8] P. Blennow, J. Hjelm, T. Klemenso, S. Ramousse, A. Kromp, A. Leonide, A. Weber, Journal of Power Sources, 196 (2011) 7117-7125.
[9] T. Klemenso, J. Nielsen, P. Blennow, A. G. Persson, T. Stegk, P. Hjalmarsson, B. H. Cristense, S. Sonderby, J. Hjelm, and S. Ramousse, ECS Transactions, 35 (2011) 369-378.
[10] N. Christiansen, S. Primdahl, M. Wandel, S. Ramousse, and A. Hagen, ECS Transactions, 57 (2013) 43-52.
[11] V. V. Krishnan, Wiley Interdisciplinary Reviews-Energy and Environment, 6 (2017).
[12] M. C. Tucker, Energy Technology, 5 (2017) 2175-2181.
[13] G. Y. Lau, M.C. Tucker, C.P. Jacobson, S.J. Visco, S.H. Gleixner, L.C. DeJonghe, Journal of Power Sources, 195 (2010) 7540-7547.
[14] M. C. Tucker, H. Kurokawa, C. P. Jacobson, L. C. De Jonghe, S. J. Visco, Journal of Power Sources, 160 (2006) 130-138.
[15] R. F. Wang, U. B. Pal, S. Gopalan, S. N. Basu, Journal of the Electrochemical Society, 164 (2017) F740-F747.
[16] M. C. Tucker, Journal of Power Sources, 369 (2017) 6-12.
[17] Y. Yoo, Y. L. Wang, X. H. Deng, D. Singh, J. G. Legoux, Journal of Power Sources, 215 (2012) 307-311.
[18] C. Metcalfe, J. Kuhn, O. Kesler, Journal of Power Sources, 243 (2013) 172-180.
[19] C. S. Hwang, C. H. Tsai, J. F. Yu, C. L. Chang, J. M. Lin, Y. H. Shiu, S. W. Cheng, Journal of Power Sources, 196 (2011) 1932-1939.
[20] Z. Y. Han, Z. B. Yang, M. F. Han, International Journal of Hydrogen Energy, 41 (2016) 10935-10941.
[21] A. M. Dayaghi, K. J. Kim, S. Kim, J. Park, S. J. Kim, B. H. Park, G. M. Choi, Journal of Power Sources, 324 (2016) 288-293.
[22] H. J. Cho, K. J. Kim, Y. M. Park, G. M. Choi, International Journal of Hydrogen Energy, 41 (2016) 9577-9584.
[23] H. J. Cho, Y. M. Park, G. M. Choi, Solid State Ionics, 192 (2011) 519-522.
[24] Y. C. Zhou, Z. C. Zhang, C. Yuan, J. L. Li, C. R. Xia, Z. L. Zhan, S. R. Wang, International Journal of Hydrogen Energy, 38 (2013) 16579-16583.
[25] E. Dogdibegovic, R. F. Wang, G. Y. Lau, M. C. Tucker, Journal of Power Sources, 410 (2019) 91-98.
[26] N. Shaigan, W. Qu, D. G. Ivey, W. X. Chen, Journal of Power Sources, 195 (2010) 1529-1542.
[27] J. W. Fergus, International Journal of Hydrogen Energy, 32 (2007) 3664-3671.
[28] M. C. Tucker, B. Carreon, J. Charyasatit, K. Langston, C. Taylor, J. Manjarrez, N. Burton, M. LaBarbera, C. P. Jacobson, ECS Transactions, 57 (2013) 503-509.
[29] R. Leah, A. Bone, M. Lankin, A. Selcuk, M. Rahman, A. Clare, L. Rees, S. Phillip, S. Mukarjee, M. Selby, ECS Transactions, 68 (2015) 95-107.
[30] A. Ansar, P. Szabo, J. Arnold, Z. Ilhan, D. Soysal, R. Costa, A. Zagst, M. Gindrat, and T. Franco, ECS Transactions, 35 (2011) 147-155.

[31] Y. Matsuzaki, I. Yasuda, Journal of the Electrochemical Society, 148 (2001) A126-A131.

[32] Y. Matsuzaki, I. Yasuda, Solid State Ionics, 132 (2000) 271-278.

[33] N. Minh, J. Mizusaki, S. C. Singhal, ECS Transactions, 78 (2017) 63-73.

[34] E. Konysheva, H. Penkalla, E. Wessel, J. Mertens, U. Seeling, L. Singheiser, K. Hilpert, Journal of the Electrochemical Society, 153 (2006) A765-A773.

[35] S.P. Jiang, X.B. Chen, International Journal of Hydrogen Energy, 39 (2014) 505-531.

[36] N. Christiansen, H. Holm-Larsen, S. Linderoth, P. H. Larsen, A.H. Hendriksen, Conference Proceedings: Energy solutions for sustainable development, Roskilde, Denmark, 2007, pp. 357-362.

[37] E. Dogdibegovic, PhD Thesis, University of South Carolina, The institutional repository of the University of South Carolina, 2017, pp. 197-211.

[38] P. Alnegren, M. Sattari, J.E. Svensson, J. Froitzheim, Journal of Power Sources, 301 (2016) 170-178.

[39] L. Sanchez, M.P. Hierro, F.J. Perez, Oxidation of Metals, 71 (2009) 173-186.

[40] J. Zurek, E. Wessel, L. Niewolak, F. Schmitz, T.U. Kern, L. Singheiser, W.J. Quadakkers, Corrosion Science, 46 (2004) 2301-2317.

[41] D. J. Young, J. Zurek, L. Singheiser, W.J. Quadakkers, Corrosion Science, 53 (2011) 2131-2141.

[42] H. E. Evans, A. T. Donaldson, T. C. Gilmour, Oxidation of Metals, 52 (1999) 379-402.

[43] A. Karimaghaloo, J. Koo, H.-S. Kang, S. A. Song, J. H. Shim, M.H. Lee, International Journal of Precision Engineering and Manufacturing-Green Technology, (2019) 1-18. Online version: https://doi.org/10.1007/s40684-019-00090-9.

[44] R.W. Johnson, A. Hultqvist, S.F. Bent, Materials Today, 17 (2014) 236-246.

[45] A. Karimaghaloo, A.M. Andrade, S. Grewal, J.H. Shim, M.H. Lee, ACS Omega, 2 (2017) 806-813.

[46] Y. Gong, D. Palacio, X. Song, R.L. Patel, X. Liang, X. Zhao, J.B. Goodenough, K. Huang, Nano Letters, 13 (2013) 4340-4345.

[47] H.J. Choi, K. Bae, S. Grieshammer, G.D. Han, S.W. Park, J.W. Kim, D.Y. Jang, J. Koo, J.W. Son, M. Martin, J.H. Shim, Advanced Energy Materials, 8 (2018) 9.